Cogging Torque Minimization in Permanent Magnet Brushless DC Motors for High-Speed Application

Seok-Myeong Jang*, Han-Wook Cho † and Dae-Joon You*

Abstract - In a permanent magnet brushless dc motor, cogging torque is produced by the magnetic attraction between the rotor mounted permanent magnets and the stator teeth. This always produces a pulsating torque ripple resulting in vibration and acoustic noise, which is detrimental to the motor performance. This paper deals with the analytical prediction of cogging torque and the various cogging torque minimization techniques as applied to a permanent magnet brushless dc motor.

Keywords: Cogging torque minimization, permanent magnet brushless dc motor, torque ripple.

1. Introduction

Permanent magnet brushless dc motors are widely used in numerous applications, such as in household electrical appliances, computer peripherals, and servo control systems, in which torque ripple and acoustic noise are the main concern. Cogging torque minimization is becoming necessary since the motor is finding its application in torque ripple to be sensitive to various applications such as electric power steering, robotics, and high-speed application, etc [1].

Cogging torque is produced, in a permanent magnet brushless machine, by the magnetic attraction between the rotor mounted permanent magnets and the stator teeth. It is the circumferential component of attractive force that attempts to maintain the alignment between the stator teeth and the permanent magnets.

For calculation of cogging torque, the airgap field is analyzed by space harmonics field analysis of magnetization and the cogging torque is computed by net lateral force acting on the teeth. Slotting effect in the airgap flux density distribution and cogging torque characteristics are analyzed by combining relative permeance [2, 3]. The relative permeance is calculated according to an assumed field pattern in which the flux crosses the magnet and the airgap in a straight line wherever a magnet faces a tooth and in a circular path, centered about the corner of a tooth, wherever a magnet faces a slot opening. The flux density of the slot region is multiplied by relative permeance.

In this paper, methods such as varying the magnet pole-arc to pole-pitch ratio, magnet strength, auxiliary slots, varying the radial shoe depth and skewing are analyzed. These methods are applied to a 4-pole, 24-slot, surface mounted permanent magnet brushless dc motor.

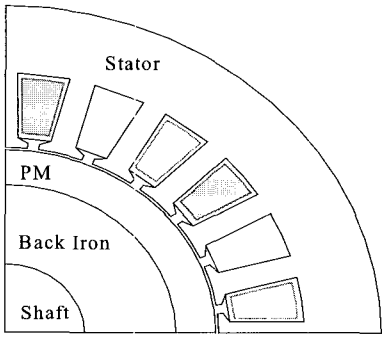

Fig. 1 Cross-section of permanent magnet brushless dc motor.

2. Analytical Prediction of Cogging Torque

The cogging torque is defined as a torque produced by magnetic forces in the circumferential direction between the stator teeth and the magnets of the rotor. Because it is superposed on the mean output torque as a fluctuating component, it can be a significant performance index of noise and vibration as well as smoothness in rotations of the rotor [1]. In this section, an analytical prediction that can be useful in the preliminary design and modification of the permanent magnet brushless dc motor is suggested.

Fig. 1 shows the cross-section of a 4-pole, 24-slot permanent magnet brushless dc motor, with a parallel magnetized permanent magnet rotor.

2.1 Relative Permeance in Airgap

In the calculation of the cogging torque, the airgap flux

† Corresponding Author: Department of Electrical Engineering, Chung nam National University, Daejeon, 305-764, Korea (hwcho@cnu.ac.kr)
* Department of Electrical Engineering, Chungnam National University, Daejeon, 305-764, Korea (smjang@cnu.ac.kr, ydjgood@cnu.ac.kr).
Received April 13, 2004 ; Accepted February 17, 2005

density with relative permeance is required only in the slot-opening regions. It is assumed that the fluxes pass on each side of the tooth circularly. The calculation of flux distribution in the slot opening region taking into account the relative permeance is shown in Fig. 2.

In order to simplify the field calculation, the following assumptions are made [2]:

a) The permeability of the iron is infinite.
b) The slots are simplified to a rectangular shape.
c) The magnetic field distribution is determined from the product of the magnetic field produced by the magnets and the relative permeance.
d) The magnetic field developed by the magnets is obtained from a 2-d solution by assuming a smooth stator surface.
e) The airgap permeance is calculated according to an assumed field pattern in which the flux crosses the magnet and the airgap in a straight line wherever a magnet faces a tooth and in a circular path, centered about the corner of a tooth, wherever a magnet faces a slot opening.

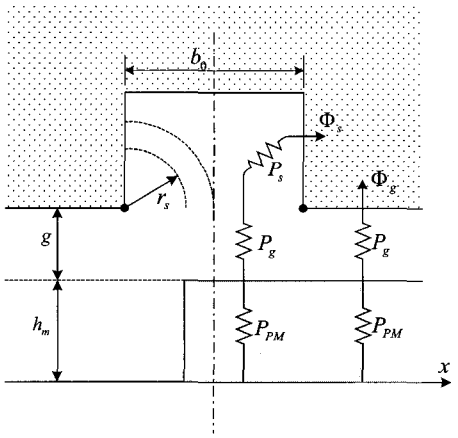

Fig. 2 Airgap representation for calculation of relative permeance

According to assumption (e) the permeance P and the relative permeance $\hat{P}$ can be calculated approximately from [2]and[3]:

$$P = \frac{\mu_0}{g + \frac{h_m}{\mu_r} + \frac{2\pi r_s}{4}} \tag{1}$$

$$\hat{P} = \frac{P}{\frac{\mu_0}{g + h_m / \mu_r}} \tag{2}$$

for $(k-1)\tau_t - b_0/2 \le x \le (k-1)\tau_t + b_0/2$

where k=1,2,... Q_s; $(\pi/\tau_p)x = p\theta$; Q_s is the number of slots, τ_p is the pole pitch; τ_t is the slot pitch; g is the airgap length; h_m is the height of the magnets. Therefore, the flux density distribution on the stator core is calculated as follows:

$$\hat{B} = \hat{P} \cdot B_{magnet} \tag{3}$$

where, $\hat{B}$ is the flux density distribution considering the relative permeance, B_{magnet} is the flux density distribution by a smooth stator surface.

2.2 Calculation of Magnetic Field

To calculate cogging torque, the airgap field is analyzed by space harmonics field analysis of magnetization and the cogging torque is computed by net lateral force acting on the teeth [3].

The flux density B and field intensity H in the airgap can be related as given in the following equation.

$$\vec{B} = \mu_0 \vec{H} \tag{4}$$

where μ_0 is the permeability of the air. Since the field intensity H can be expressed in terms of a magnetic scalar potential, ϕ is defined as

$$\vec{H} = -\nabla\phi \tag{5}$$

The magnetic scalar potential distribution in the airspace is governed by Laplace's equation. In the permanent magnet regions it is governed by quasi-Poissonian equation. i.e.,

$$\frac{\partial^2\phi}{\partial r^2} + \frac{1}{r}\frac{\partial\phi}{\partial r} + \frac{1}{r^2}\frac{\partial\phi^2}{\partial\theta^2} = 0 \tag{6}$$

and

$$\frac{\partial^2\phi}{\partial r^2} + \frac{1}{r}\frac{\partial\phi}{\partial r} + \frac{1}{r^2}\frac{\partial\phi^2}{\partial\theta^2} = \frac{M_r}{r\mu_r} \tag{7}$$

Therefore, the airgap flux density is represented by Forier series as

$$B_{magnet} = \sum_{n=1,3,..}^{\infty} 4\frac{M_n}{\mu_r}\frac{np}{(np)^2-1}\left(\frac{R_i}{R_o}\right)^{np-1}\cos np\theta \cdot \left[\frac{(np-1)R_o^{2np} + 2R_m^{np+1}R_0^{np-1} - (np+1)R_m^{2np}}{\frac{\mu_r+1}{\mu_r}\left\{R_i^{2np} - R_m^{2np}\right\} - \frac{\mu_r-1}{\mu_r}\left\{R_o^{2np} - R_i^{2np}(R_m/R_o)^{2np}\right\}}\right] \tag{8}$$

in which when $np=1$,

$$B_{magnet} = 2M_1 \cos np\theta \cdot \left[\frac{R_o^2 - R_m^2 + R_m^2 \ln(R_o/R_m)^2}{\frac{\mu_r+1}{\mu_r}\{R_i^2 - R_m^2\} - \frac{\mu_r-1}{\mu_r}\{R_o^2 - R_i^2(R_m/R_o)^2\}} \right] \quad (9)$$

where, p is the number of pole pairs, M_n is the magnetization, R_i and R_o are shaft and magnet outer radius, and R_s is stator inner radius, respectively.

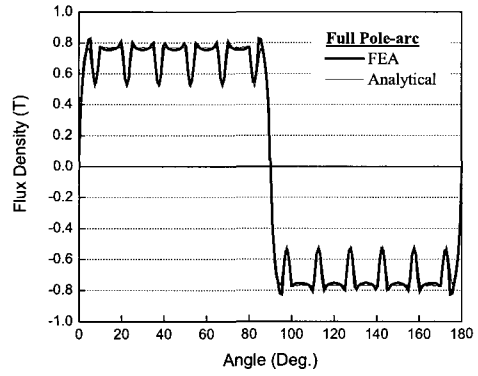

Fig. 3 Airgap flux distribution of full-pole arc model

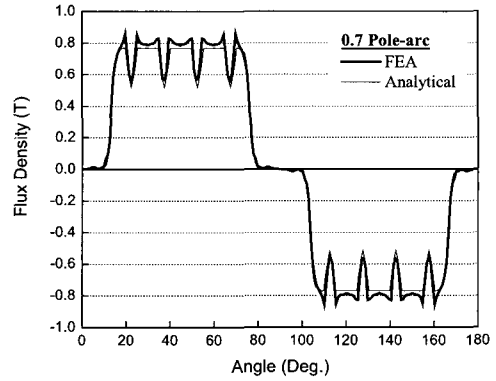

Fig. 4 Airgap flux distribution of 0.7-pole arc model

where, n is the space harmonic order, p is the pole pairs, and μ_r is the recoil permeability of the permanent magnet. R_o, R_i and R_m is the rotor outer radius, stator inner radius and the permanent magnet inner radius, respectively. The magnetization M is [2] in the following:

$$M = \sum_{n=1,3,..}^{\infty} 2M_n \cos np\theta \quad (10)$$

and

$$M_n = B_r \alpha_p \frac{\sin\frac{n\alpha_p\pi}{2}}{\frac{n\alpha_p\pi}{2}} \quad (11)$$

where B_r is the remanence, and α_p is the ratio of pole-arc to pole-pitch of the magnets.

Figs. 3 and 4 show the airgap flux density distribution of the analysis model with full/0.7 pole-arc to pole-pitch ratio. The results are shown in to be in good agreement with those obtained from the finite element analysis (FEA).

2.3 Calculation of Cogging Torque with Magnet Shifting Technique

Fig. 5 indicates the magnet shift technique for calculation of cogging torque. Fig. 6(a) is the simple stator teeth/slot shape, and (b) and (c) are the starting and ending point of the permanent magnet of the rotor.

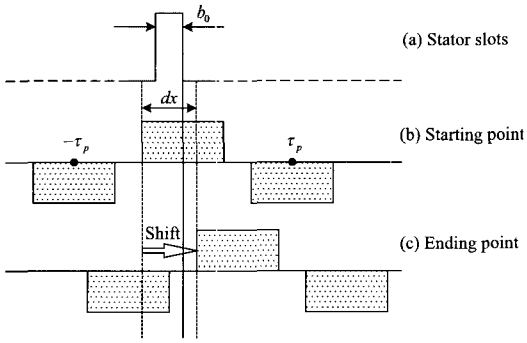

Fig. 5 Magnet shift technique for calculation of cogging torque.

If the distance by which one pole-pair is shifted relative to another pole-pair is d_x, the resultant magnetization is [2]:

$$M = \sum_{n=1,2,..}^{\infty} M_n \left\{ \cos n\frac{\pi}{\tau_p}x + (-1)^{n+1}\cos n\frac{\pi}{\tau_p}(x-d_x) \right\} \quad (12)$$

where $(\pi/\tau_p)x=p\theta$, M_n is still given by equation (6). However, the harmonic order n is now given by n=1,2,3,... Therefore, it can be replaced in equation (7) with

$$M_n \left\{ \cos n\frac{\pi}{\tau_p}x + (-1)^{n+1}\cos n\frac{\pi}{\tau_p}(x-d_x) \right\} \quad (13)$$

The magnetic field produced by the magnets when they are shifted is obtained. Hence the cogging torque can be evaluated by equation (10). Cogging torque is caused by the non-constant airgap permeance due to slotting. The torque is produced by the fluxes that enter the teeth walls.

Cogging torque expression results.

$$T_c = \sum_{k=0}^{Q_s} l_a \int_0^{b_0} \left(\frac{B_{rb_1}^2 - B_{rb_2}^2}{2\mu_0} \right) r_t dr_s \qquad (14)$$

where, l_a is the stator stack length, b_0 is the slot opening width, and $r_t = R_i + r_s$.

A comparison between the analytically predicted cogging torque variation with rotor position angle and corresponding result from FEA for the analysis model is shown in Fig. 6.

3. Cogging Torque Minimization Techniques

The cogging torque is defined as a torque produced by

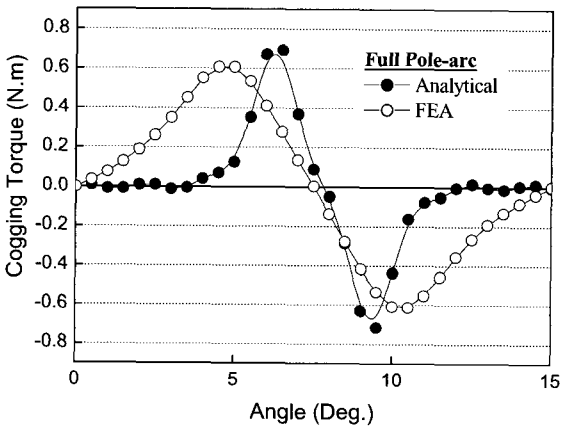

Fig. 6 Comparison of analytically and finite element predicted cogging torque waveform.

magnetic forces in the circumferential direction between the stator teeth and the rotor magnets.

In this paper, methods such as varying the magnet pole-arc to pole-pitch ratio, varying the magnet strength, shifting magnet, auxiliary slots, varying the radial shoe depth and the skew are analyzed. The machine and the minimization techniques are simulated using a two-dimensional finite element analysis package. In the following sections, the minimization techniques and the results of the analysis are described.

3.1 Magnet Pole-Arc

The magnet arc is a particularly important parameter in regard to the level of cogging torque. It has been found that the optimum ratio of pole-arc to pole-pitch ratio for minimizing the cogging torque occurs without much reduction in the back-EMF amplitude or degradation to its harmonic contents [4, 5].

Figs. 7 and 8 show the effect of pole-arc to pole-pitch ratio on cogging torque waveform and amplitude of cogging torque. It is assumed that the magnets are identical and have parallel magnetization. As shown in the plot, the cogging torque is very sensitive to variation in the magnet angle. Hence, it imposes tight manufacturing tolerances if used for minimizing cogging torque.

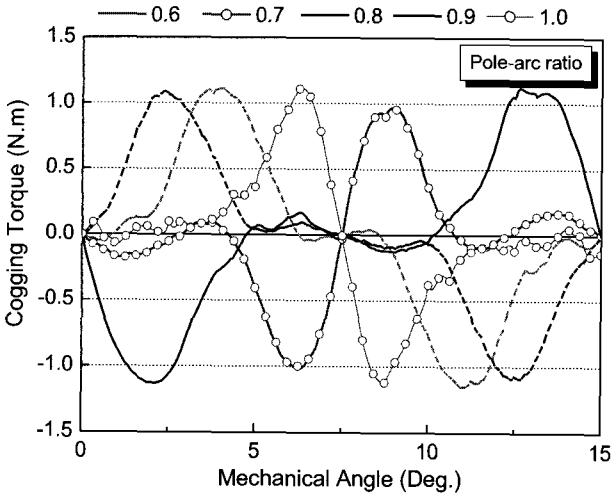

Fig. 7 Effect of pole-arc to pole-pitch ratio on cogging torque waveform.

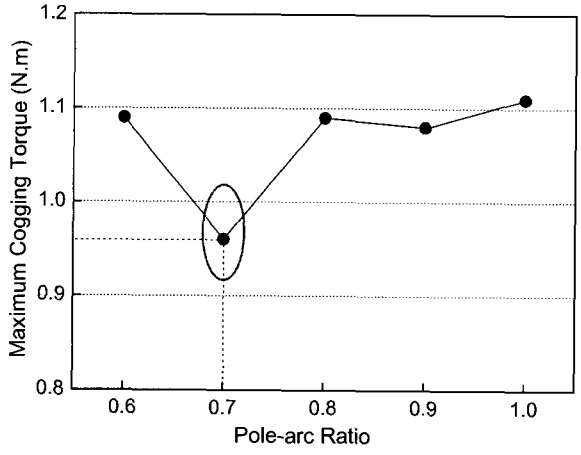

Fig. 8 Effect of pole-arc to pole-pitch ratio on amplitude of cogging torque.

3.2 Magnet Strength

Fig. 9 indicates one cycle of cogging torque for a variation in magnet remanence. The magnet remanence is varied from 0.7 to 1.2 Tesla in increments of 0.1 Tesla. Fig. 10 shows the amplitude of maximum cogging torque for a variation in magnet remanence. As seen by the figure, the peak value of cogging torque varies directly with the change in magnet remanence, while the shape of the curve

remains unchanged [4].

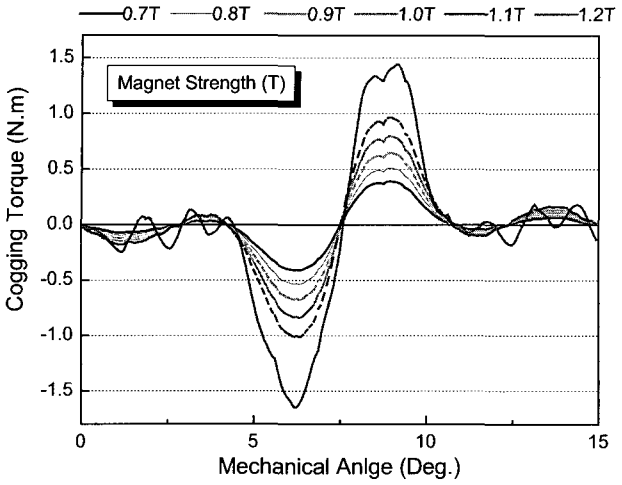

Fig. 9 Effect of magnet remanence on cogging torque waveform.

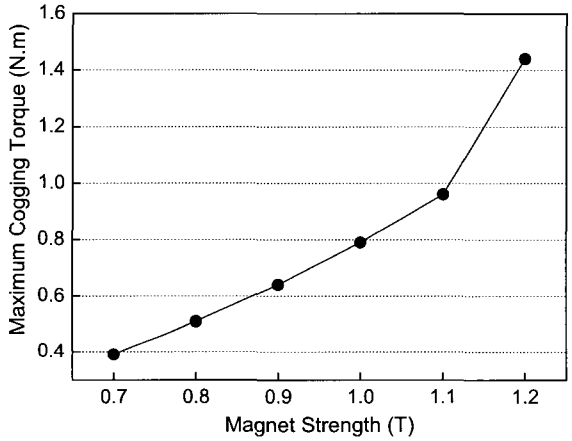

Fig. 10 Effect of magnet remanence on amplitude of cogging torque.

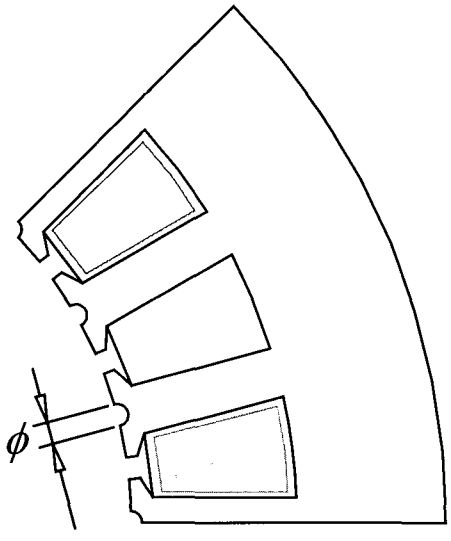

Fig. 11 Auxiliary slots for analysis model

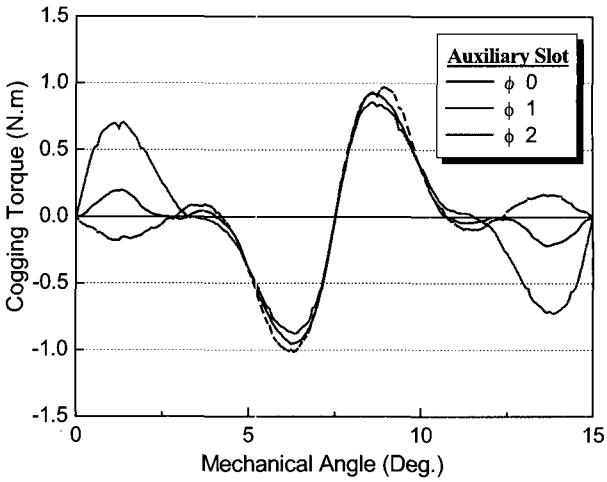

Fig. 12 Effect of auxiliary slots on cogging torque waveform.

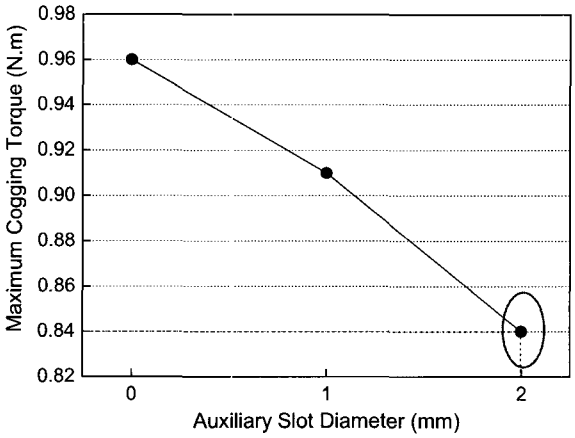

Fig. 13 Effect of auxiliary slots on amplitude of cogging torque.

3.3 Auxiliary Slots

The auxiliary slots do not have copper winding. Furthermore, they are only for additional cogging torque removal technique in the stator. It is known that the fundamental harmonic of the cogging is the minimum common multiple of the number of poles and the number of slots. With the introduction of auxiliary slots, the order of the fundamental harmonics of the Fourier decomposition is increased, thus, the cogging torque should reduce. Fig. 11 shows the auxiliary slots for the analysis model.

Figs. 12 and 13 present the effect of the cogging torque of the analysis model with auxiliary slots.

3.4 Varying the Radial Shoe Depth

Since magnetic flux enters a ferromagnetic material perpendicular to its surface, the tangential components of

attractive force are greatest at the sides of the stator teeth. Varying the radial shoe depth changes the magnitude of cogging torque by altering the distribution of the tangential components of attractive force in the area at the side of the shoe [4].

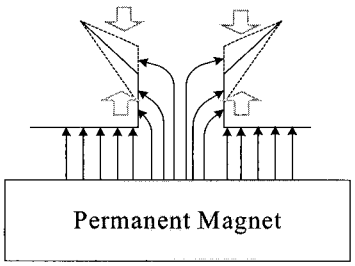

Fig. 14 Variation of the radial shoe depth

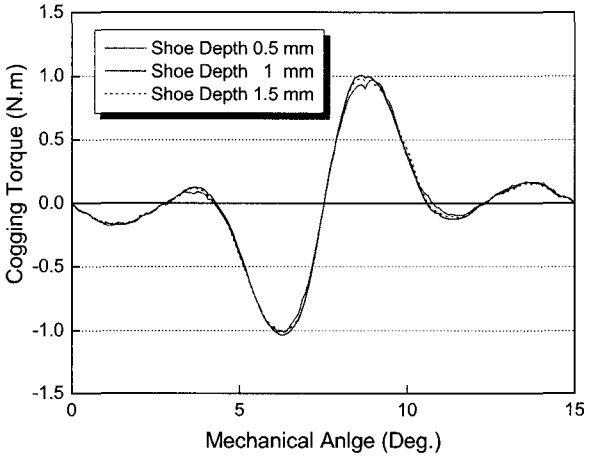

Fig. 15 Effect of variation of the radial shoe depth on cogging torque waveform.

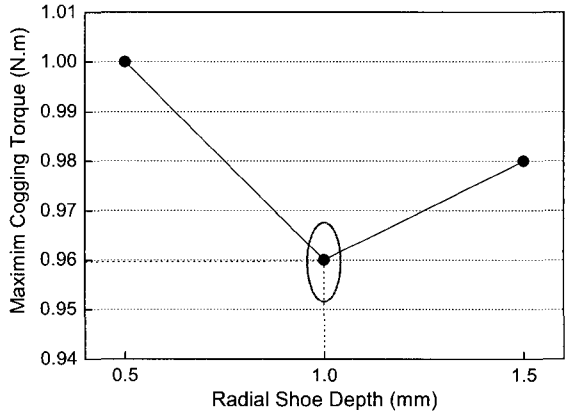

Fig. 16 Effect of variation of the radial shoe depth on amplitude of cogging torque.

Fig. 15 shows one cycle of cogging torque for a variation in the radial shoe depth. The radial shoe depth is varied from 0.5 mm to 1.5 mm increments. As illustrated in the figure, there is a small change in the magnitude of the cogging torque curve.

Fig. 16 indicates the maximum value of cogging torque versus the radial shoe depth. The radial shoe depth that produces the minimum cogging torque is approximately one millimeter.

3.5 Skewing

A well-known method to reduce the cogging torque is the skewing of the stator slots or of the permanent magnets, obtaining the same results. The stator skewing makes the automatic slot filling impossible. Hence, rotor magnet skewing is more popular than stator skewing. Fig. 17 shows the ideal rotor magnet skewing.

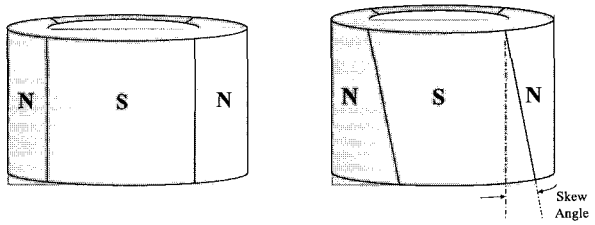

Fig. 17 Skewing of the rotor magnet.

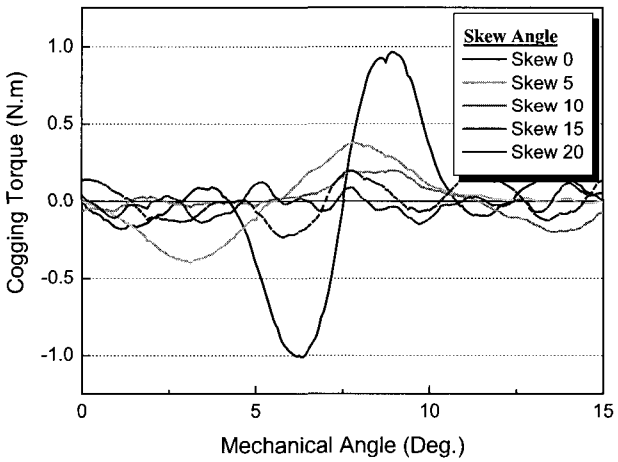

Fig. 18 Effect of skewing on cogging torque waveform.

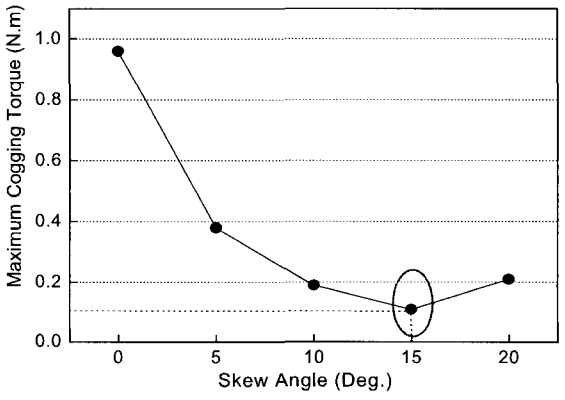

Fig. 19 Effect of skewing on amplitude of cogging torque.

Fig. 18 presents the effect of the cogging torque of the analysis model for a variation in the rotor magnet skewing angle. The skewing angle is varied from 0 to 15 degrees in increments of 5 degrees. As seen by the figure, the peak value of cogging torque varies directly with the change in the skewing angle. Fig. 19 demonstrates the effect of skewing on amplitude of the cogging torque. The skewing angle that produces the minimum cogging torque is approximately 15 mechanical degrees. That is one slot pitch of the stator.

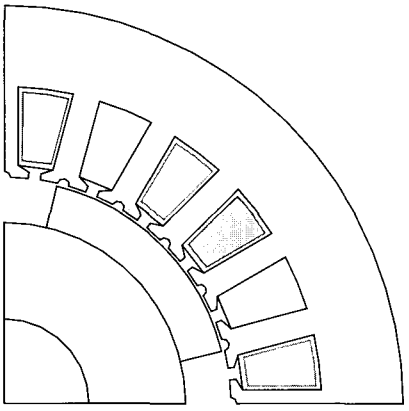

Fig. 20 Cross-section of proposed brushless DC motor considering the various techniques for minimizing the cogging torque.

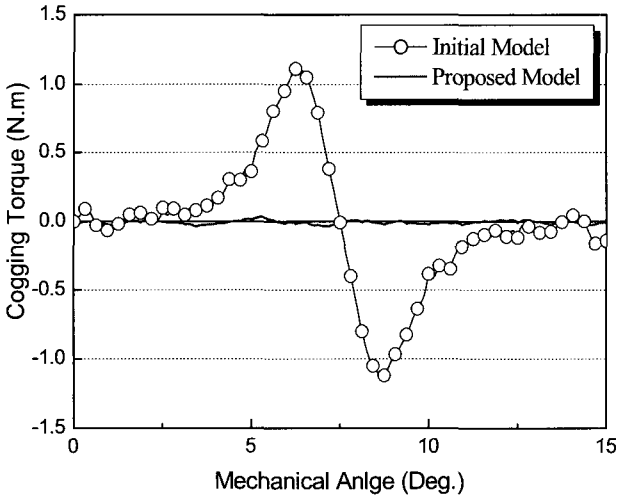

Fig. 21 The cogging torque plot for proposed motor.

3.6 Minimizing the Cogging Torque of the Permanent Magnet Brushless DC motor

Fig. 20 shows the 4-pole permanent magnet brushless dc motor considering the various techniques for minimizing the cogging torque in sections 3.1 to 3.5. The stator has an auxiliary slot and the rotor magnets are skewed by one slot pitch with 0.7 pole-arc to pole-pitch ratio. The diameter of an auxiliary slot is 2mm, and radial shoe depth is 1mm. Fig 21 presents the cogging torque plot for a proposed motor. As seen in the figure, the cogging torque is reduced significantly.

4. Conclusion

Considering the effect of slotting, the analytical calculation of the permanent magnetic field and cogging torque are discussed, based on the space harmonic field method. Analytical results are verified with FE results. Moreover, the various techniques for minimizing the cogging torque of the permanent magnet brushless dc motor have been presented.

Acknowledgements

This work was financially supported by MOCIE through the IERC program of Korea.

References

[1] Mohammad S. Islam, Sayeed Mir, Tomy Sebastian, "Issues in reducing the cogging torque of mass-produced permanent magnet brushless dc motor," *IEEE Trans. Indust. Applicat.*, vol. 40, pp. 813-820, May/June 2004.

[2] Z.Q.Zhu and D.Howe, "Analytical prediction of the cogging torque in radial-field permanent magnet brushless motors," *IEEE Trans. Magn.*, vol. 28, pp. 1371-1374, March 1992.

[3] Gyu-Hong Kang, Jung-Pyo Hong and Gyu-Tak Kim, "Analysis of cogging torque in interior permanent magnet motor by analytical method," *KIEE International Transactions on EMECS*, vol. 11-B, pp. 1-8.

[4] C. Studer, A. Keyhani, T. Sebastian, S. K. Murthy, "Study of cogging torque in permanent magnet machines," *IAS Annual Meeting Proc.* pp. 42-49, Oct. 4-9, 1997.

[5] N. Bianchi and S. Bolognani, "Design techniques for reducing the cogging torque in surface-mounted PM motors," *IEEE Trans. Ind. Applicat.*, vol. 38, pp. 1259-1265, Sept./Oct. 2002.

[6] K.Ng, Z.Q.Zhu and D.Howe, "Open-circuit field distribution in a brushless motor with diametrically magnetized PM rotor, accounting for slotting and eddy current effects," *IEEE Trans. Magn.*, vol. 32, pp. 5070-5072, Sept. 1997.

[7] Z.Q.Zhu, K.Ng and D.Howe, "Design and analysis of high-speed brushless permanent magnet motors," *Electrical Machines and Drives*, pp. 381-385, Sept. 1997.

[8] Janne Nerg, Markku Niemelä, Juha Pyrhönen, Jarmo Partanen, "FEM calculation of rotor losses in a medium speed direct torque controlled PM synchronous motor at different load conditions," *IEEE Trans. Magn.*, vol. 38, pp. 5070-5072, Sept. 1997.

Seok-Myeong Jang

He was born in Korea in 1949. He received his B.E, M.S., and Ph.D. degrees from Hanyang University in 1976, 1978, and 1986, respectively. Currently, he is a Professor in the Department of Electrical Engineering at Chungnam National University. He worked as a Visiting Researcher in the Department of Electrical Engineering at Kentucky University in 1989. He is presently Vice President of KIEE and President of the EMECS Society. His field of interest includes the design and application of Linear Machines, Permanent Magnet Synchronous Machines, and Linear Oscillating Actuators.
Tel: +82-42-821-5658

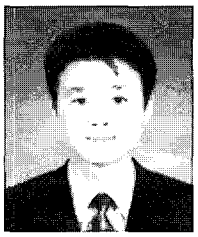

Han-Wook Cho

He was born in Korea in 1976. He received his B.S. and M.S. degrees in Electrical Engineering from Chungnam National University in 2002 and 2004, respectively. He is currently working toward his Ph.D. in the Dept. of Electrical Engineering at Chungnam National University. His research interests include the design of permanent magnet type electric machines and drives.
Tel: +82-42-821-7608

Dae-Joon You

He was born in Korea in 1976. He received his B.S. and M.S. degrees in Electrical Engineering from Chungnam National University in 2003 and 2005, respectively. He is currently working toward his Ph.D. in the Dept. of Electrical Engineering at Chungnam National University. His research interests include the design and control of PM linear motors.
Tel: +82-42-821-7608